Exact and geometrical optics energy trajectories in twisted beams

M V Berry[1] and K T McDonald[2]

[1] H H Wills Physics Laboratory, Tyndall Avenue, Bristol BS8 1TL, UK
[2] Joseph Henry Laboratories, Princeton University, Princeton, NJ 08544, USA

Abstract
Energy trajectories, that is, integral curves of the Poynting (current) vector, are calculated for
scalar Bessel and Laguerre–Gauss beams carrying orbital angular momentum. The trajectories
for the exact waves are helices, winding on cylinders for Bessel beams and hyperboloidal
surfaces for Laguerre–Gauss beams. In the geometrical optics approximations, the trajectories
for both types of beam are overlapping families of straight skew rays lying on hyperboloidal
surfaces; the envelopes of the hyperboloids are the caustics: a cylinder for Bessel beams and
two hyperboloids for Laguerre–Gauss beams.

Keywords: Poynting, rays, diffraction

1. Introduction

One of several ways to depict optical fields is by the trajectories of energy flow, that is, the lines everywhere tangent to the Poynting vector. Here we will describe light by a scalar wave $\psi(r)$, constructed for example from the vector potential [1, 2], or representing a single field component, or simply regarded as a physical model in which polarization effects are neglected. Then the Poynting vector can be chosen parallel to the current, that is, the expectation value of the local momentum operator, namely

$$P(r) = \text{Im}\,\psi^*(r)\,\nabla\psi(r) = |\psi(r)|^2\,\nabla\arg\psi(r). \quad (1.1)$$

The second equality expresses the fact that in vacuum $P(r)$ is orthogonal to the wavefronts (contour surfaces of phase $\arg\psi$). $P(r)$ is an important ingredient in calculating the orbital angular momentum of the field [3], and forces on small particles in the field. In quantum physics, the trajectories are the streamlines in the Madelung [4] hydrodynamic interpretation, later regarded as paths of quantum particles in the Bohm–de Broglie interpretation [5].

For optical beams, where there is a well-defined propagation direction z, it is natural to represent the trajectories using z as a parameter, and the field using cylindrical polar coordinates $\{r, \phi, z\}$. Then, writing $P(r)$ in the form

$$P(r) = F(r)\left\{v_r(r)\,e_r + v_\phi(r)\,e_\phi + e_z\right\}, \quad (1.2)$$

the trajectories are the integral curves of P, to be obtained by solving the differential equations

$$\frac{\mathrm{d}r(z)}{\mathrm{d}z} \equiv r'(z) = v_r(r(z)),$$
$$\frac{\mathrm{d}\phi(z)}{\mathrm{d}z} \equiv \phi'(z) = \frac{v_\phi(r(z))}{r(z)}. \quad (1.3)$$

Our aim here is to understand the energy trajectories for Bessel and Laguerre–Gauss beams carrying orbital angular momentum ('twisted beams'), which are of current interest theoretically and experimentally, building on and extending previous studies [6, 7]. We emphasize a fundamental point, central to the understanding of energy flow: the equation (1.1) can be interpreted in two quite different ways, both of which we will employ in the following.

In the first (sections 2 and 3), $\psi(r)$ is the exact solution of the relevant wave equation; then $P(r)$ has the advantage that it represents without approximation the flow described by the wave equation.

In the second (sections 4 and 5), the lines of $P(r)$ represent the rays of geometrical optics, which although approximate carry the intuitive appeal that their envelopes are the caustic surfaces on which the field is most intense. In this case, $\psi(r)$ represents one of possibly several locally plane waves that are superposed to create the total field. When points in the field are reached by several geometrical rays, the corresponding pattern of trajectories overlap, unlike the exact Poynting trajectories of the total field, which are

uniquely defined at each point. $\boldsymbol{P}(\boldsymbol{r})$ depends nonlinearly on $\psi(\boldsymbol{r})$, so the superposition of trajectories is different from the trajectories of the superposition.

In vacuum or any homogeneous medium, the geometrical rays are straight lines. This is an immediate consequence of Snell's law (or, more abstractly, Hamilton's equations), according to which rays bend only if there is a variation of refractive index. The straightness is not immediately obvious from the algebraic formulae describing the rays, but will be confirmed by showing that they satisfy the following equations, expressing the vanishing of the curvature $|\boldsymbol{r}' \times \boldsymbol{r}''|/|\boldsymbol{r}'|$:

$$r\phi'' + 2r'\phi' = 0, \qquad r'' - r\phi'^2 = 0. \qquad (1.4)$$

By contrast, the trajectories of the exact Poynting vector are usually curved.

For the beams we study here, it turns out, unexpectedly, to be easier to calculate the exact Poynting trajectories than the geometrical rays, which require knowledge of the asymptotics of Bessel and Laguerre functions.

2. Bessel beams: exact Poynting flow lines

These beams are exact solutions of the Helmholtz equation, defined [8, 9] by

$$\psi_l(\boldsymbol{r}) = \exp\left\{ i\left(\sqrt{k^2 - q^2}z + l\phi \right) \right\} J_l(qr), \qquad (2.1)$$

in which l is the angular momentum quantum number, k the free-space wavenumber and q the magnitude of the transverse component of the wavevector of the plane waves comprising the beam.

Since the Bessel function is real, only the first factor contains the phase $\arg \psi$ which according to (1.1) generates the Poynting vector, and (1.2) gives

$$v_r = 0, \qquad v_\phi = \frac{l}{r\sqrt{k^2 - q^2}}. \qquad (2.2)$$

The trajectories are determined by the differential equations (1.3), which can be trivially solved to give

$$r = \text{constant}, \qquad \phi = \phi_0 + \frac{l}{r^2\sqrt{k^2 - q^2}}z. \qquad (2.3)$$

This describes a two-parameter family of helices (figure 1) filling space. Each helix can be defined by the point $\{r, \phi_0\}$ where it pierces the plane $z = 0$. The pitch of the helices with radius r is

$$\Delta z = \frac{2\pi r^2 \sqrt{k^2 - q^2}}{l}, \qquad (2.4)$$

so the wider helices are more longitudinally stretched.

3. Laguerre–Gauss beams: exact Poynting flow lines

These beams are exact solutions of the paraxial wave equation, defined [3] by

$$\psi_{l,p}(\boldsymbol{r}) = \exp\{i(kz + l\phi)\} \exp\left\{ -\frac{\rho^2}{2w(\zeta)} \right\} \frac{\rho^{|l|}}{w(\zeta)^{|l|+1}} \rho^{|l|}$$

$$\times \left(\frac{w(-\zeta)}{w(\zeta)} \right)^p L_p^{|l|}\left(\frac{\rho^2}{1 + \zeta^2} \right). \qquad (3.1)$$
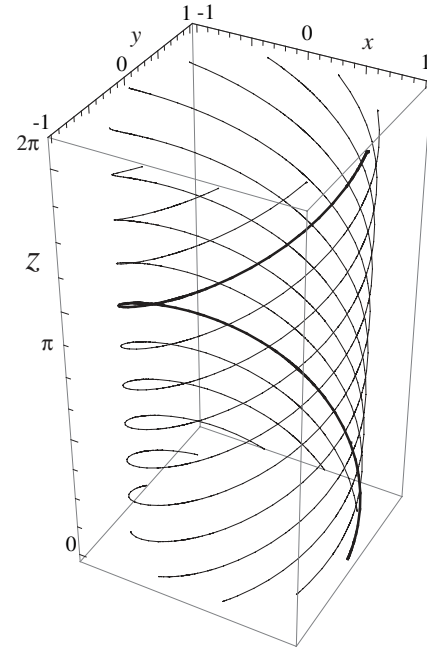

Figure 1. Exact Poynting trajectories for Bessel beams. The trajectories, which fill space, are helices wound on cylinders corresponding to different radii r, and the helices on different cylinders have different pitches Δz, according to (2.4).

Here $L_p^{|l|}$ denotes the Laguerre polynomial [10], with indices representing the angular momentum quantum number l and radial node number p (that is, $p + 1$ radial bright rings), the scaled coordinates are defined in terms of the waist radius w_0 ($1/e$ radius of the intensity $|\psi|^2$) by

$$\{x, y, z\} \equiv \{\xi w_0, \eta w_0, k w_0^2 \zeta\}, \qquad \rho \equiv \sqrt{\xi^2 + \eta^2}, \quad (3.2)$$

and

$$w(\zeta) = 1 + i\zeta. \qquad (3.3)$$

For convenience we will henceforth consider only positive l, and so will omit the modulus signs. (The paraxial approximation to Bessel beams, in which $\sqrt{k^2 - q^2}$ in (2.1) is approximated by $k - q^2/2k$ can be obtained from (3.1) in the limit $p \to \infty$, using the identity (22.15.2) in [10].)

Since L_p^l is real, it does not contribute to the phase, which is therefore given by

$$\arg \psi_{l,p} = kz + l\phi + \frac{\rho^2 \zeta}{2(1 + \zeta^2)} + G(\zeta). \qquad (3.4)$$

$G(\zeta)$ denotes the Gouy phase, which enters through the factors involving powers of $w(\zeta)$ and does not affect the shape of the trajectories apart from a slight longitudinal stretching; in what follows, we will neglect this effect. Identification of the Poynting components via (1.2) gives

$$v_\rho = \frac{\rho \zeta}{1 + \zeta^2}, \qquad v_\phi = \frac{l}{\rho}, \qquad (3.5)$$

and thence the differential equations (1.4) determining the trajectories:

$$\rho'(\zeta) = \frac{\rho(\zeta)\zeta}{1 + \zeta^2}, \qquad \phi'(\zeta) = \frac{l}{\rho(\zeta)^2}. \qquad (3.6)$$
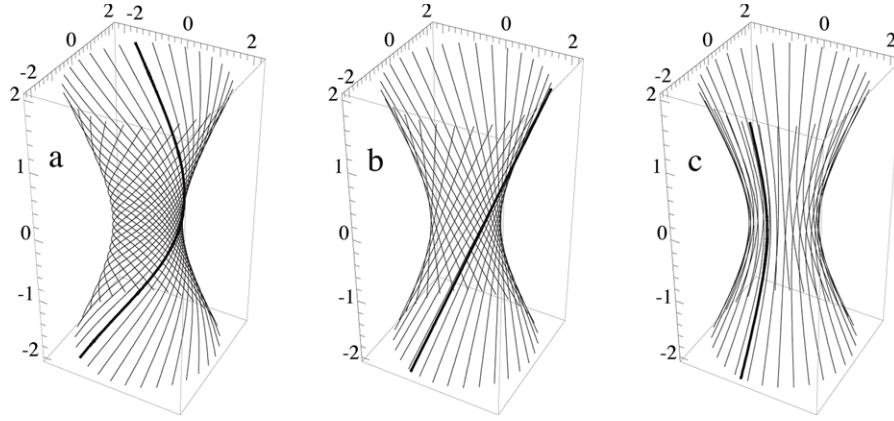
Figure 2. Exact Poynting trajectories for Laguerre–Gauss beams. The trajectories, which fill space, wind on hyperboloidal surfaces corresponding to different values of ρ_0^2/l. (a): $\rho_0^2/l = 0.5$; (b): $\rho_0^2/l = 1$; (c) $\rho_0^2/l = 10$. The total rotation angle of the trajectory, $\Delta\phi$ (equation (3.8)) is unrelated to the Gouy phase. The trajectories are all curved except when $\rho_0^2/l = 1$ (as in (b)).

Equation (3.5) determines the local skew angle of the Poynting vector, that has recently been measured directly [11].

The solutions are easily found, and give the trajectory passing through the point ρ_0, ϕ_0 in the waist plane $\zeta = 0$ as

$$\rho(\zeta) = \rho_0\sqrt{1 + \zeta^2}, \qquad \phi(\zeta) = \phi_0 + \frac{l}{\rho_0^2}\tan^{-1}\zeta. \quad (3.7)$$

These are curves wound on hyperboloids (figure 2); the windings get slower as $|\zeta|$ increases, and the total angle turned through between $\zeta = -\infty$ and $+\infty$ is

$$\Delta\phi = \frac{\pi l}{\rho_0^2}. \quad (3.8)$$

Note that this rotation does not involve the Gouy phase.

The trajectories are generally not straight, because one of the curvature components in (1.4) is non-zero:

$$r\phi'' + 2r'\phi' = 0, \qquad r'' - r\phi'^2 = \frac{1 - (l/\rho_0^2)^2}{(1 + \zeta)^{3/2}}. \quad (3.9)$$

However, the hyperboloid with $\rho_0\sqrt{l}$ is exceptional: its trajectories are straight lines. For the special beam with $p = 0$, this was noted in [6] and interpreted in terms of skew rays (see also figure 6 of [12]), which as we will see in sections 4 and 5 is in fact the correct geometrical-optics interpretation for all beams. This insight corrected an earlier error in an important paper [13], which had claimed that the energy trajectories are continuously rotating helices. However, the lines calculated in [6] for general Laguerre–Gauss beams, with $p \neq 0$, are contours in which the direction of the Poynting vector is associated with regions of large magnitude $|\psi|$, which are not energy trajectories in the usual sense (1.3), that is, integral curves of the Poynting field.

4. Bessel beams: geometrical-optics rays

In the geometrical-optics regime of large l, the Bessel function $J_l(qr)$ in (2.1) is exponentially small if $qr < l$. For

$qr > l$, there are radial oscillations, described by the Debye approximations [10]

$$
\begin{aligned}
&J_l(qr) \\
&\approx \sqrt{\frac{2}{\pi}} \frac{\cos\left\{\sqrt{q^2r^2 - l^2} - l\tan^{-1}\left(\sqrt{q^2r^2 - l^2}/l\right) - \frac{1}{4}\pi\right\}}{(q^2r^2 - l^2)} \\
&\qquad (l \gg 1, qr > l).
\end{aligned} \quad (4.1)
$$

The oscillations correspond to the interference of geometrical rays, which we treat separately by regarding the cosine as the sum of two complex exponentials (this is equivalent to the decomposition into outgoing and ingoing Hankel functions: $J_l = (H_l^{(1)} + H_l^{(2)})/2$).

From (2.1), the total phase of each contribution is

$$
\begin{aligned}
\arg\psi_{l,\pm} = z\sqrt{k^2 - q^2} + l\phi \pm \left(\sqrt{q^2r^2 - l^2} - \right. \\
\left. \times\, l\tan^{-1}(\sqrt{q^2r^2 - l^2}/l)\right),
\end{aligned} \quad (4.2)
$$

so the Poynting components are

$$v_r = \pm\frac{\sqrt{q^2r^2 - l^2}}{r\sqrt{k^2 - q^2}}, \qquad v_\phi = \frac{l}{r\sqrt{k^2 - q^2}}, \quad (4.3)$$

and the trajectories are the solutions of

$$r'(z) = \pm\frac{\sqrt{q^2r(z)^2 - l^2}}{r(z)\sqrt{k^2 - q^2}}, \qquad \phi'(z) = \frac{l}{r(z)\sqrt{k^2 - q^2}}. \quad (4.4)$$

It is convenient to specify the trajectories by the height z_0 at their 'turning radius', where $r'(z_0) = 0$, that is $r = l/q$. Thus

$$\int_{q/l}^{r(z)} \frac{\mathrm{d}r\, r}{\sqrt{q^2r^2 - l^2}} = \frac{(z - z_0)}{\sqrt{k^2 - q^2}}, \quad (4.5)$$

leading to the explicit solutions

$$r(z) = \frac{q}{\sqrt{k^2 - q^2}}\sqrt{(z - z_0)^2 + \frac{l^2(k^2 - q^2)}{q^4}} \quad (4.6)$$

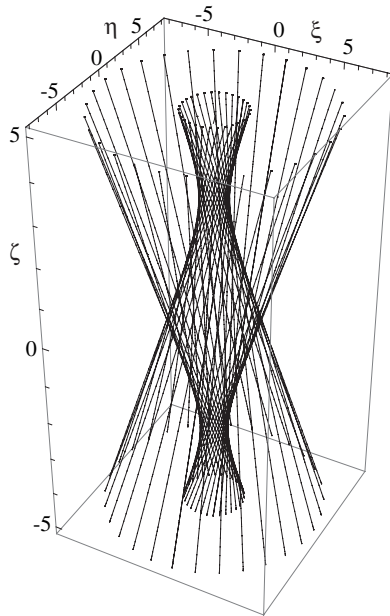$$\phi(z) = \phi_0 + \tan^{-1}\left\{\frac{(z - z_0)q^2}{l\sqrt{k^2 - q^2}}\right\}.$$

3

Figure 3. Geometrical rays for Bessel beams, calculated from (4.8) with $\zeta_0 = +3$ and $\zeta_0 = -3$ for a range of starting angles ϕ_0. All rays are straight, and turn by π between $\zeta = \pm\infty$. The totality of rays for all ϕ_0, ζ_0 fill space outside the caustic at $\rho = 1$, that is $r = l/q$.

With the dimensionless variables

$$r \equiv \frac{l}{q}\rho, \qquad z \equiv \frac{l\sqrt{k^2 - q^2}}{q^2}\zeta, \qquad (4.7)$$

the trajectories take the convenient form

$$\rho(\zeta) = \sqrt{(\zeta - \zeta_0)^2 + 1}, \qquad \phi = \phi_0 + \tan^{-1}(\zeta - \zeta_0). \qquad (4.8)$$

These expressions satisfy (1.4), confirming that the geometrical trajectories are straight lines. For fixed ζ_0, the trajectories for different ϕ_0 again form a set of skew rays lying on hyperboloidal surfaces (figure 3). The totality of these hyperboloids fills the space outside the cylinder $\rho = 1$, that is $r = l/q$, which is the caustic (figure 4) where $J_l(qr)$ is large for large l. For $l = 0$, the caustic surface degenerates to the axis, which becomes a focal line, through which pass the trajectories: lines, no longer skew, with inclination angle $\arcsin(q/k)$.

5. Laguerre–Gauss beams: geometrical-optics rays

In geometrical optics, interpreted as the regime where waves can be represented as the superposition of locally plane waves, l and p are simultaneously large. To study this, we need some facts about the function

$$g_{l,p}(x) \equiv \exp\left(-\tfrac{1}{2}x\right) x^{l/2} L_p^l(x), \qquad (5.1)$$

involving the Laguerre polynomial $L_p^l(x)$; derivations are outlined in the appendix. $g(x)$ oscillates in a certain range $x_- < x < x_+$, and decays exponentially outside this range. The limits are given by

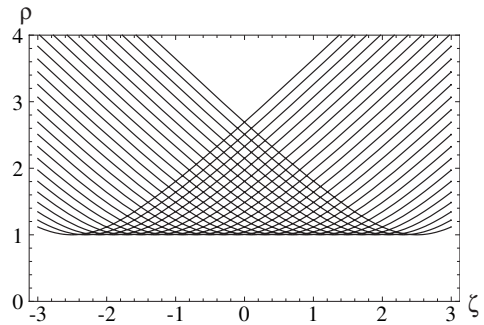$$x_\pm = l + 2p + 1 \pm \sqrt{(l + 2p + 1)^2 - (l - 1)^2} \approx l s_\pm\left(\frac{p}{l}\right), \qquad (5.2)$$

Figure 4. Geometrical Bessel rays: radial coordinate $\rho(\zeta)$ for different ζ_0, showing the caustic at $\rho = 1$.
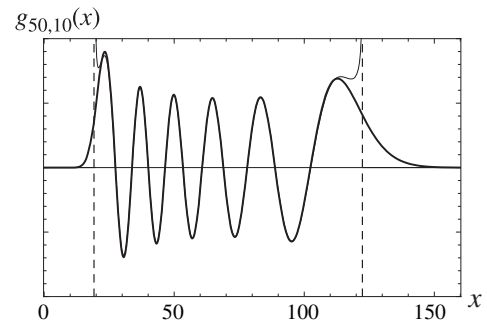

Figure 5. Asymptotic behaviour of Laguerre functions. Thick curve: $g_{l,p}(x) \equiv \exp(-\tfrac{1}{2}x)x^{l/2}L_p^l(x)$ for $l = 50$, $p = 10$; thin curve: asymptotic approximation (A.4)–(A.6) in oscillatory region; dashed lines: the theoretical limits $x_- = 19.62$ and $x_+ = 122.38$.

in which the functions $s_\pm(u)$ are

$$s_\pm(u) = 1 + 2u \pm 2\sqrt{u^2 + u} = \frac{1}{s_\mp(u)}. \qquad (5.3)$$

Figure 5 illustrates this behaviour.

As with the Bessel beams, we can regard the oscillation as the decomposition of the real Laguerre function into two complex functions, that is

$$L_p^l(x) \approx X_{l,p}(x) + \left(X_{l,p}(x)\right)^*, \qquad (5.4)$$

which are locally exponential in form. The rate of oscillation (local radial wavenumber) is

$$\frac{d}{dx} \arg X_{l,p}(x) = -\frac{\sqrt{(x_+ - x)(x - x_-)}}{2x}. \qquad (5.5)$$

Thus, introducing the physical dimensionless variables ρ and ζ as in (3.1), the Poynting vector components are

$$v_\rho = \frac{1}{1 + \zeta^2}\left(\rho\zeta \pm \frac{\sqrt{(\rho_+^2 - \rho^2)(\rho^2 - \rho_-^2)}}{\rho}\right), \qquad (5.6)$$

$$v_\phi = \frac{l}{\rho},$$

in which
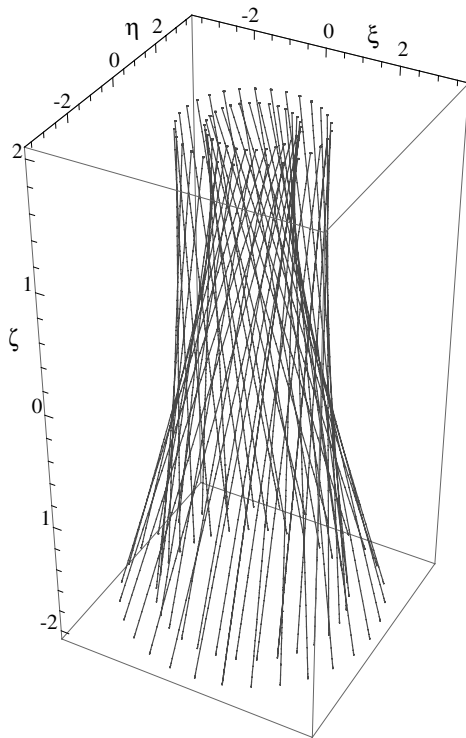
$$\rho_\pm^2 = l s_\pm(1 + \zeta^2). \qquad (5.7)$$

4

Figure 6. Geometrical rays $\{\rho_\pm(\zeta), \phi_\pm(\zeta)\}$ for Laguerre–Gauss beams, calculated from (5.9) and (5.10) with $\zeta_0 = 1.5$ and a range of starting angles ϕ_0, and $x_+/l = 4$, $x_-/l = 0.25$. All rays are straight, and turn by π between $\zeta \pm \infty$. The totality of rays for all ϕ_0, ζ_0 fill space between the two caustic surfaces shown in figure 7.

Thus, the equations determining the trajectories are

$$\rho'(\zeta) = \frac{1}{1+\zeta^2}$$
$$\times \left(\rho(\zeta)\zeta \pm \frac{\sqrt{(\rho_+^2 - \rho(\zeta)^2)(\rho(\zeta)^2 - \rho_-^2)}}{\rho(\zeta)} \right),$$
$$\phi' = \frac{l}{\rho(\zeta)^2}. \tag{5.8}$$

Somewhat surprisingly, the graphs of $\rho(\zeta)$ for different trajectories are again hyperbolas. Considerable algebra confirms the following expressions, conveniently specified by the height ζ_0 where the trajectory comes closest to the axis, and corresponding to the two signs in (5.8):

$$\rho_\pm(\zeta) = \sqrt{\frac{l}{A_\pm\left(\frac{p}{l}, \zeta_0\right)} \left[A_\pm\left(\frac{p}{l}, \zeta_0\right)^2 (\zeta - \zeta_0)^2 + 1 \right]} \tag{5.9}$$
$$\phi_\pm(\zeta) = \phi_0 + \tan^{-1}\left\{ A_\pm\left(\frac{p}{l}, \zeta_0\right)(\zeta - \zeta_0) \right\},$$

in which

$$A_\pm(u, \zeta_0) = \frac{s_+ + s_- \pm \sqrt{(s_+ - s_-)^2 - 4\zeta_0^2}}{2\left(1 + \zeta_0^2\right)}$$
$$= \frac{1 + 2u \pm \sqrt{4u\left(1 + u\right) - \zeta_0^2}}{\left(1 + \zeta_0^2\right)}. \tag{5.10}$$
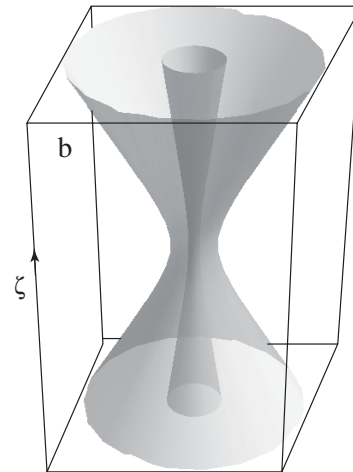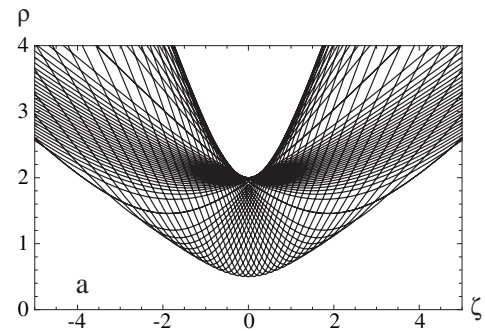

Figure 7. (a) Geometrical Laguerre–Gauss rays: radial coordinate $\rho_\pm(\zeta)$ for different ζ_0, showing the caustics at $\rho_\pm = \frac{x_\pm}{l}\sqrt{(1 + \zeta^2)}$. (b) Caustic surfaces.

It is clear that all trajectories have closest approaches to the axis in the range of heights $|\zeta_0| < 2\sqrt{\frac{p}{l}(1 + \frac{p}{l})}$. Again, use of (1.4) confirms that the rays are straight.

Figure 6 shows the $+$ and $-$ ray families for a typical ζ_0. Again they lie on hyperboloids, with the difference from the Bessel beam that now there are two hyperboloids for each ζ_0, and the dimensions of the hyperboloids depend on ζ_0. The envelope of all the hyperboloids is a caustic surface with two sheets (figure 7), both themselves hyperboloids, given by

$$\rho_{\text{caustic},\pm} = \sqrt{ls_\pm\left(1 + \zeta^2\right)}, \tag{5.11}$$

corresponding to large values of the Laguerre polynomials at the extremes (5.2) of the oscillatory range. The totality of all the skew rays on all the hyperboloids fills the space between the two caustic surfaces.

6. Concluding remarks

The results reported here show that the energy trajectories of Bessel and Laguerre–Gauss beams can be calculated exactly, and show somewhat richer behaviour than might have been anticipated. Especially significant are the differences between the Poynting vector lines of the exact beams (generally curved)
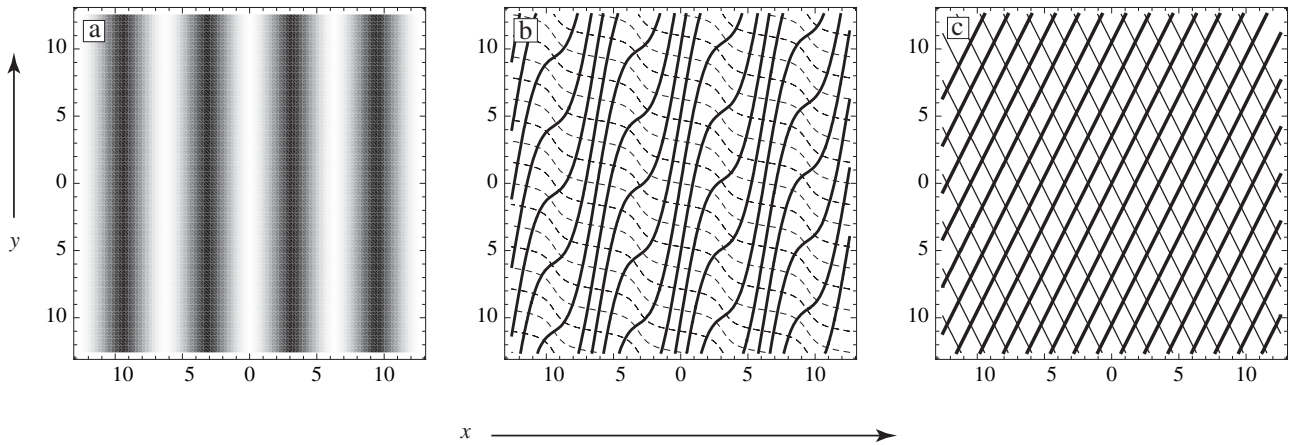
Figure 8. Representations of the unequal superposition (6.1) of two plane waves with $a = b = 1/2$. (a) Intensity $|\psi|^2$. (b) Thick curves: Poynting trajectories $\operatorname{Im}\psi^*\nabla\psi$; dashed curves: wavefronts $\arg\psi = $ constant. (c) Geometrical-optics rays: thick lines represent the right-travelling (stronger) wave and the thin lines represent the left-travelling (weaker) wave.

and those of the component ray families in the geometrical-optics approximation (overlapping families of straight skew rays).

Nevertheless, the behaviour is not typical. The Bessel functions and Laguerre polynomials are real and therefore have zeros on nodal surfaces (hyperboloidal in form), in contrast to typical complex wavefunctions, whose zeros are lines (of phase singularity, also called wavefront dislocations or optical vortices). Associated with this is the fact that the locally plane waves that are superposed in the oscillatory regions of the beams are equal in amplitude. Typically, the waves are of unequal amplitude, and then the exact Poynting trajectories are wavy. A simple—almost trivial—example is the superposition of two plane waves equally inclined to the y axis:

$$\psi(x, y) = \exp\{i(y + ax)\} + b\exp\{i(y - ax)\}. \quad (6.1)$$

The intensity

$$|\psi(x, y)| = 1 + b^2 + 2b\cos 2ax, \quad (6.2)$$

possesses maxima (figure 8(a)) along lines parallel to the common propagation direction y. This contrasts with the Poynting trajectories, which when parametrized by the height y_0 where they intersect the y axis are given by

$$y - y_0 = \frac{1}{a(1 - b^2)}\left((1 + b^2)x + \frac{b}{a}\sin 2ax\right). \quad (6.3)$$

These are wavy lines (figure 8(b)) slanted towards the direction of the more intense plane wave component in (6.1). And of course these in turn are very different from the superposition of the two families of geometrical rays (families of parallel straight lines, figure 8(c)) representing the two component waves. The particular wave (6.1) has no vortices. When vortices are present, trajectories generally spiral slowly into and out of them [14]—another feature that does not occur for the axial vortices in the beams considered here.

We expect other families of beams (for example, Hermite–Gauss or Mathieu) to exhibit similar behaviour, that is, curved Poynting trajectories for the exact waves and, in the geometrical-optics approximation, skew families of straight rays enveloping caustic surfaces.

Acknowledgment

Appendix. Laguerre asymptotics

We include this section to present the most compact derivation of results we need; for a rigorous treatment, and references to the extensive mathematical literature on Laguerre polynomials, see [15].

From the Rodrigues formula [10] for the Laguerre polynomials, the function $g_{l,p}(x)$ in (5.1) can be written as a pth derivative, which in turn can be expressed as a contour integral:

$$
\begin{aligned}
g_{l,p}(x) &\equiv \exp\left(-\tfrac{1}{2}x\right)x^{l/2}L_p^l(x) \\
&= \frac{\exp\left(\tfrac{1}{2}x\right)x^{-l/2}}{p!}\frac{d^p}{dx^p}\left(\exp(-x)x^{p+l}\right) \\
&= \frac{\exp\left(\tfrac{1}{2}x\right)x^{-l/2}}{2\pi i}\oint\frac{dz}{(z-x)^{p+1}}\exp(-z)z^{p+l} \\
&= \frac{\exp\left(\tfrac{1}{2}x\right)x^{-l/2}}{2\pi i}\oint dz\exp\{F(z, x)\},
\end{aligned} \quad (A.1)
$$

where the contour is a loop surrounding $z = x$, and

$$F(z, x) \equiv -z + (p + l)\log z - (p + 1)\log(z - x). \quad (A.2)$$

In the geometrical-optics regime (large l and p), F is large and the integrand is fast-varying, the contour can be deformed so as to pass through saddle points, where the exponential is locally stationary; the integral is dominated by contributions from these points. There are two saddles, given by

$$
\frac{\partial F}{\partial z} = 0 \Rightarrow z = z_\pm(x)
$$

$$
= \tfrac{1}{2}\left[x + l - 1 \pm \sqrt{(x - l + 1)^2 - 4(p + 1)x}\right]. \quad (A.3)
$$

Complex exponential contributions to $g_{l,p}(x)$ correspond to complex saddles, in which the argument in the square root

in (A.3) is negative. It is easy to confirm that this implies that x must lie between the limits (5.2).

The function $g_{l,p}(x)$ is now given by the standard saddle-point method [16, 17] (local Gaussian expansion of the integrand) as

$$
g_{l,p}(x) \approx -\exp\left(\tfrac{1}{2}x\right) x^{-l/2}
$$
$$
\times \sqrt{\frac{2}{\pi}}\, \mathrm{Im}\left[\frac{\exp\{F(z_+(x),x)\}}{\sqrt{-\partial^2 F(z=z_+(x),x)/\partial z^2}} \right]
$$
$$
(x_- < x < x_+), \tag{A.4}
$$

or, more explicitly (after some algebra),

$$
g_{l,p}(x) \approx -\sqrt{\frac{2}{\pi}}\, \frac{(p+l)^{\frac{1}{2}(p+l)+\frac{1}{4}} \exp\left\{-\tfrac{1}{2}l\right\}}{p^{\frac{1}{2}p+\frac{1}{4}} \left[(x_+ - x)(x - x_-)\right]^{1/4}} \sin\mu
$$
$$
(x_- < x < x_+), \tag{A.5}
$$

where

$$
\mu = \mathrm{Im}\, F(z_+(x),x) - \frac{1}{2}\arg\left[-\frac{\partial^2 F(z=z_+(x),x)}{\partial z^2} \right]. \tag{A.6}
$$

Figure 5 shows how accurately these formulae describe the Laguerre function in its oscillatory range.

The rate of oscillation (local wavenumber) is

$$
\frac{\mathrm{d}}{\mathrm{d}x}\arg X_{l,p}(x) \approx \frac{\mathrm{d}}{\mathrm{d}x}\mathrm{Im}\, F(z_+(x),x)
$$
$$
= \frac{\partial}{\partial x}\mathrm{Im}\, F(z_+(x),x) = \mathrm{Im}\frac{(p+1)}{z_+(x) - x}, \tag{A.7}
$$

which with (A.3) leads to the formula (5.5) that we used to obtain the Poynting vector components.

As the order p of the derivative in (A.1) increases, so does the range over which the Laguerre function $g_{l,p}(x)$ oscillates (cf (5.2)), leading in the limit to the radial oscillations of the Bessel beams. This is an example of the universal phenomenon that high derivatives of almost every smooth function are locally sinusoidal; for a general theory, see [18].

References

[1] Green H S and Wolf E 1953 A scalar representation of electromagnetic fields *Proc. Phys. Soc.* A **66** 1129–37
[2] Wolf E 1959 A scalar representation of electrromagnetic fields: II *Proc. Phys. Soc.* **74** 269–80
[3] Allen L, Padgett M J and Babiker M 1999 The orbital angular momentum of light *Prog. Opt.* **39** 291–372
[4] Madelung E 1926 Quantentheorie in hydrodynamische form *Z. Phys.* **40** 322–6
[5] Holland P 1993 *The Quantum Theory of Motion. An Account of the de Broglie Bohm Causal Interpretation of Quantum Mechanics* (Cambridge: Cambridge University Press)
[6] Padgett M J and Allen L 1995 The Poynting vector in Laguerre–Gauss laser modes *Opt. Commun.* **121** 36–40
[7] Allen L, Barnett S M and Padgett M J 2003 *Optical Angular Momentum* (Bristol: Institute of Physics Publishing)
[8] Durnin J 1987 Exact solutions for nondiffracting beams. I. The scalar theory *J. Opt. Soc. Am.* **4** 651–4
[9] Durnin J, Miceli J J Jr and Eberly J H 1987 Diffraction-free beams *Phys. Rev. Lett.* **58** 1499–501
[10] Abramowitz M and Stegun I A 1972 *Handbook of Mathematical Functions* (Washington: National Bureau of Standards)
[11] Leach J, Keen S, Padgett M J, Saunter C and Love G D 2006 Direct measurement of the skew angle of the Poynting vector in a helically phased beam *Opt. Express* **14** 11919
[12] Courtial J and Padgett M J 2000 Limit to the orbital angular mnomentum per unit energy in a light beam that can be focussed onto a small particle *Opt. Commun.* **173** 269–74
[13] Allen L, Beijersbergen M W, Spreew R J C and Woerdman J P 1992 Orbital angular momentum and the transformation of Gauss–Laguerre modes *Phys. Rev. Lett.* A **45** 8185–9
[14] Berry M V 2005 Phase vortex spirals *J. Phys. A: Math. Gen.* L745–51
[15] Bosbach C and Gawronski W 1998 Strong asymptotics for Laguerre polynomials with varying weights *J. Comput. Appl. Math.* **99** 77–89
[16] Wong R 1989 *Asymptotic Approximations to Integrals* (New York: Academic)
[17] de Bruijn N G 1958 *Asymptotic Methods in Analysis* (Amsterdam: North-Holland) (1981 reprinted by Dover Books)
[18] Berry M V 2005 Universal oscillations of high derivatives *Proc. R. Soc.* A **461** 1735–51